Measurement of mass-gated neutron multiplicity for the ^{48}Ti + ^{208}Pb reaction at 57.4 MeV excitation energy

Meenu Thakur,[*] B. R. Behera,[†] Ruchi Mahajan, Gurpreet Kaur, Priya Sharma, Kushal Kapoor, and Kavita Rani
Department of Physics, Panjab University, Chandigarh 160014, India

P. Sugathan, A. Jhingan, N. Saneesh, R. Dubey, A. Yadav, A. Chatterjee, and M. B. Chatterjee
Inter University Accelerator Centre, Aruna Asaf Ali Marg, New Delhi 110067, India

Neeraj Kumar and S. Mandal
Department of Physics and Astrophysics, University of Delhi, New Delhi 110007, India

S. K. Duggi
Department of Nuclear Physics, Andhra University, Visakhapatnam 503003, India

A. Saxena and S. Kailas
Nuclear Physics Division, Bhabha Atomic Research Centre, Mumbai 400085, India

Santanu Pal
CS - 6/1, Golf Green, Kolkata 700095, India (Formerly with VECC, Kolkata)

The neutron emission in coincidence with the fragments have been investigated for the ^{48}Ti + ^{208}Pb reaction populating the near superheavy compound nucleus ^{256}Rf at an excitation energy of 57.4 MeV. The National Array of Neutron Detectors facility is used for a precise determination of the prescission (M_n^{pre}) and postscission (M_n^{post}) neutron multiplicities as a function of fission observables. A moving source fitting procedure has been adopted to deduce M_n^{pre} and M_n^{post}. The variation of M_n^{pre} with the mass-split and total kinetic energy (TKE) of the fission fragments have been studied to understand the fission dynamics of ^{256}Rf. It is observed that M_n^{pre} increases from the value of 1.66 ± 0.07 to 2.23 ± 0.07 with transition from the asymmetric to the symmetric mass region. M_n^{pre} is also found to increase with the decrease in TKE, which is probably due to the neutron emission during the acceleration time of the fission fragments in this heavy system. The experimental results for neutron multiplicity have also been compared with the theoretical predictions from the statistical model calculations. From this comparison, the value of reduced dissipation strength for the ^{256}Rf nucleus is found to be $(13.0 \pm 1.0) \times 10^{21}$ s^{-1} and a fission delay time of $(67.3^{+5.3}_{-3.9}) \times 10^{-21}$ s has also been estimated. For the spontaneous fission of ^{256}Rf, the extracted average neutron multiplicity M_n^{sf} is found to be 4.4 ± 1.0 which is in good agreement with the recently reported value for the ^{258,260}Rf isotopes.

I. INTRODUCTION

The synthesis of superheavy elements (SHEs) and understanding its reaction dynamics is an active field in nuclear physics. Predictions of an island of SHEs, with an enhanced stability owing to the shell effects [1] has triggered the experimental efforts to investigate the SHEs. Recently, the limit to produce SHEs has been pushed to $Z = 118$ through the progressive experimental attempts by various groups [2–4]. An adequate understanding of the fission dynamics of the SHEs is essential to maximize their survival probability, through the optimal selection of the projectile-target combinations and

the suitable bombarding energies. These studies are rather challenging as the survival probability of SHEs is strongly inhibited due to the interplay of equilibrated and dynamical nonequilibrated fission processes. The equilibrated fission [true fusion-fission (FF)] process comes from the symmetric fission of a compact compound nucleus (CN) formed after the full equilibration in all degrees of freedom. In nonequilibrated fission processes, after the amalgamation of colliding particles, complete equilibration does not take place in all the degrees of freedom and the formed dinuclear system prematurely segregates into asymmetric mass fragments. The quasifission (QF) [5,6], fast fission [7], pre-equilibrium fission (PEF) [8], and deep-inelastic collision (DIC) [9] are categorized as the nonequilibrated fission processes. For the sake of brevity, all the nonequilibrated fission processes are referred to as QF in this paper. The QF mechanism demonstrates a complex

---
[*]meenu.thakuroct@gmail.com
[†]Corresponding author: bivash@pu.ac.in

behavior in the fission dynamics of SHEs, which strongly depends on the entrance channel properties of the interacting nuclei namely mass asymmetry (or charge product), deformation, and magicity [10–12]. The presence of QF hinders the fusion of heavy nuclei and reduces the fusion cross sections to picobarn levels. Therefore, it is essential to experimentally check the various factors affecting the CN formation.

Various experimental probes, viz., angular distribution, mass distribution (MD), mass-energy distribution (MED), and mass-angle distribution (MAD), of the fission fragments have been employed to disentangle the QF and FF processes [5,6,13,14]. It was, however, observed that the symmetric valley region of the fragment masses receives the mixed contribution from QF and FF processes while approaching the heavier mass region. Thus, it is cumbersome to disentangle the two processes in such cases. QF and FF processes, however, follow different reaction trajectories during the evolution of a composite system, resulting in different traveling timescales of FF and QF from the contact point to the scission point. Further, the prescission neutron multiplicity directly depends on the traveling timescales of the trajectories from the contact point to the scission point and hence it can be considered as a clock for fission timescales. Therefore, the prescission neutron multiplicity may be considered as an additional probe for analyzing the reaction mechanism of the systems for which MD, MAD, and MED fail to distinguish the QF and FF processes [15,16].

The experimental data for the fragmentation dynamics and neutron multiplicity measurements in the superheavy and near-superheavy region is rather scarce. Further, it is also essential to systematically study the neutron multiplicities coming from different mass cuts of the fragments going from symmetric to asymmetric region, as it helps in determination of the timescale of reaction process. In this experiment, we have studied the MD, MED, MAD, mass-gated, and energy-gated neutron multiplicities, and neutron angular distributions for the ^{48}Ti + ^{208}Pb reaction populating the near-superheavy nucleus ^{256}Rf at an excitation energy of 57.4 MeV. These measurements offer a key insight into the fission dynamics of the ^{256}Rf nucleus. The choice of this system is made since the CN formation is assured for one of its isotope [17]. In this heavy system, QF is anticipated to occur along with true FF due to its large charge product ($Z_1 Z_2$, where Z_1 and Z_2 are the atomic numbers of projectile and target nuclei respectively). Recently, the results for the MD, MED, and MAD of the fission fragments produced in the reaction ^{48}Ti + ^{208}Pb have been reported which confirmed the substantial presence of QF processes in this heavy system [18]. In the present paper, we have used the neutron multiplicity measurements to further elucidate the fission dynamics of the ^{256}Rf nucleus by estimating the fission timescales. Very limited amount of work has been reported in literature on the neutron angular distribution measurements. With the advent of the multidetector setup, National Array of Neutron Detectors (NAND) facility [19], it is possible to measure the neutron angular distributions for the same system, more precisely for a wide range of angular positions. These measurements provide the fragment-neutron angular correlations to separate the pre- and postscission components of neutron multiplicities. Also, it is well established that fission is dissipative in nature [20]. A large number of experimental and theoretical studies have been carried out to identify and estimate the magnitude of nuclear dissipation in heavy-ion-induced reactions. Such work in the superheavy region is limited. In the current paper, estimation of dissipation strength of the ^{256}Rf is also presented. The paper is structured as follows: The experimental details are described in Sec. II, followed by a description of the data analysis strategy and the results in Sec. III. In Sec. IV, the statistical model calculations are discussed. Finally, the outcomes of the analysis are summarized and concluded in Sec. V.

II. EXPERIMENTAL DETAILS

The experiment was performed using the 15UD Pelletron + LINAC accelerator and NAND facility at Inter University Accelerator Centre (IUAC), New Delhi. Thin ^{208}Pb targets (251 μg/cm^2) [21] with carbon backing (20 μg/cm^2) were bombarded with a pulsed beam of ^{48}Ti having energy of 275 MeV to populate the near superheavy CN ^{256}Rf. Targets, with backing foil facing the beam, were mounted on the target ladder placed at the center of the scattering chamber of the NAND. The target ladder was tilted to an angle of 40° with respect to the beam axis in order to minimize the energy loss of fission fragments inside the target and shadowing to the position-sensitive multiwire proportional counters (MWPC). The intensity and repetition rate of the beam were 0.7 pnA and 250 ns respectively.

For the detection of fission fragments, two large-area (5″ × 3″) MWPCs [22] were used. MWPCs were placed on movable arms on each side of the beam axis at a distance of 25 cm from the center of the target inside the scattering chamber. Both the MWPCs were centered at polar angles (θ) of 73° (azimuthal angle, $\phi = 0°$) and 54° ($\phi = 180°$) respectively, and were operated at 4 mbar pressure of isobutane gas throughout the experiment. The angular acceptance of both the MWPCs was ±14.25° in the θ direction and ±8.67° in the ϕ direction. Two silicon surface barrier detectors (SSBD) kept at an angle of ±12.5° relative to the beam direction were used to monitor the beam flux. The hit pattern on X and Y planes of MWPC was constructed using the delay-line readout method. These X and Y position spectra were calibrated using the known positions of the edges of the active areas of the MWPCs when the events were recorded in noncoincidence mode. The elastically scattered events were used to calibrate the time-of-flight (TOF) spectrum of the fission fragments.

The neutrons emitted in coincidence with the fission fragments were detected using the NAND array consisting of 100 BC501A organic liquid scintillators. All the neutron detectors were of identical active volume of 5″ × 5″ and each was coupled to a photomultiplier tube of 5″ (PMT Model Hamamatsu R4144). These detectors were mounted at a radial distance of 175 cm from the target and installed in the circular hubs of a geodesic dome structure truncated 80 cm above the floor level. Using these hubs, eight rings were formed around the scattering chamber. The lowest ring was located 15° below the reaction plane ring. The remaining six rings were lying above the reaction plane ring with an angular separation of 15° between the two adjacent rings. In the reaction plane ring, 16 detectors were placed at the angles ranging from 18°
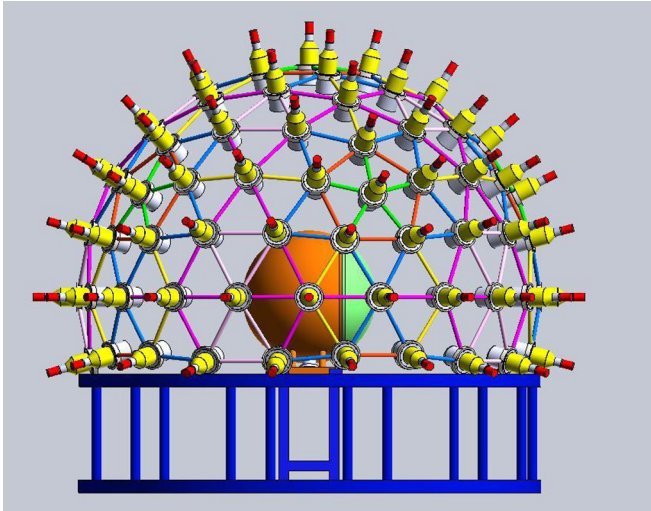
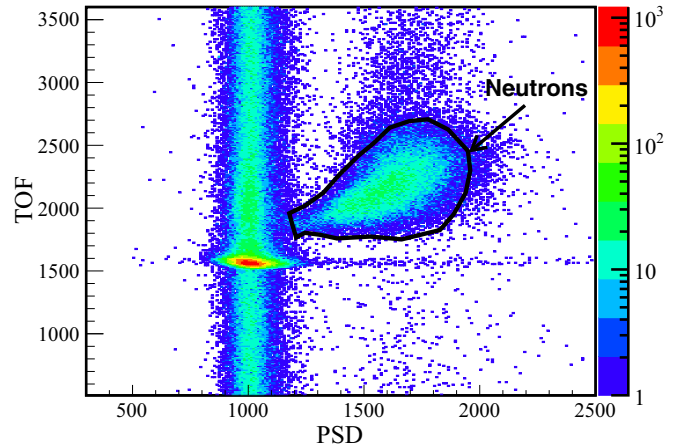FIG. 1. The pictorial view of the NAND array at IUAC.

FIG. 2. Two-dimensional plot of TOF vs PSD used to separate the neutrons from the γ's. The neutron lobe is outlined using a black solid line.

to 342°. The remaining 84 detectors were positioned at the different angles in the out of plane rings. Figure 1 shows the pictorial view of the NAND array. The calibration of neutron detectors was performed using the light output corresponding to the Compton edge of the standard γ-ray sources ^{137}Cs, ^{22}Na, and ^{60}Co [23]. With this calibration, the hardware threshold of the neutron detectors was kept at a value of 120 keV equivalent-electron (keVee). In order to limit the γ background reaching the neutron detectors, the beam dump was installed at a distance of 4 m downstream from the target. The beam dump was properly shielded with borated paraffin blocks and lead sheets. Pulse shape discrimination (PSD) based on the zero crossover technique [24] and TOF technique were employed to discriminate neutrons and γ's. The neutron TOF was deduced by considering the prompt-γ-ray peak of TOF spectrum as the time reference and then converted into the neutron energy.

The efficiency of the neutron detector was experimentally obtained by measuring the neutron energy spectrum from the spontaneous fission of a ^{252}Cf source. The ^{252}Cf was placed at the target position. To detect maximum fission events, the MWPC was kept in the close vicinity of ^{252}Cf. The MWPC was operated under the same conditions as maintained during the experiment. For the TOF spectrum, the start signal was provided by the timing signal of the MWPC and the stop signal was generated from the neutron detector. The neutron energy deduced from the calibrated TOF was gated with the neutron lobe shown in Fig. 2. Further, the derived energy spectrum was gated with the MWPC positions and the energy loss signal to efficiently select events from fission only. Afterward, the neutron energy spectra in the laboratory frame were transformed into the center-of-mass frame. The Maxwellian neutron energy spectrum of the ^{252}Cf is given as

$$\frac{dN}{dE} = \sqrt{E_n} \exp\left(-\frac{E_n}{T}\right), \tag{1}$$

where E_n is the neutron energy. T is the temperature of the neutron source and its value is 1.42 MeV for the ^{252}Cf [25].

Finally, the intrinsic efficiency of the neutron detector was determined by taking ratio of the experimentally measured energy to the Maxwellian predicted energy spectrum. The obtained efficiencies were then compared with the Monte Carlo simulated values from the FLUKA particle transport and interaction code [26]. Figure 3 indicates a good agreement between the experimental and simulated efficiencies of the neutron detector.

III. DATA ANALYSIS AND RESULTS

The main objective of the data analysis is to extract the mass and total kinetic energy of the fission fragments and to study the correlation between these binary events and the emitted neutrons. During experiment, the event rate was 0.003 neutron per fission event. Total neutrons collected in the neutron
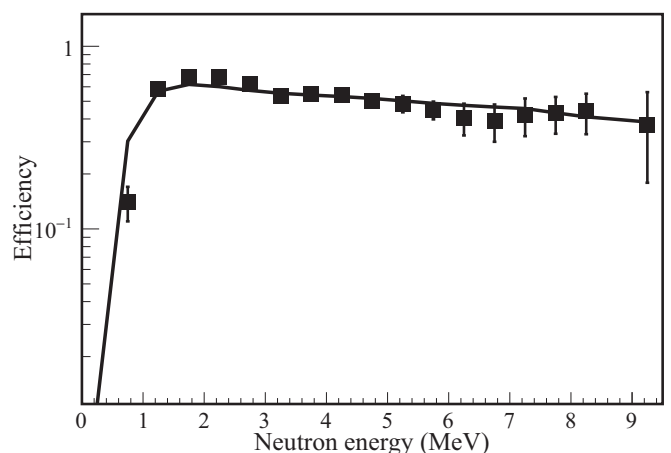

FIG. 3. Comparison of the experimentally deduced neutron efficiency (filled square) with the one obtained using Monte Carlo simulation code FLUKA (solid line) at 120 keV electron equivalent detection threshold.
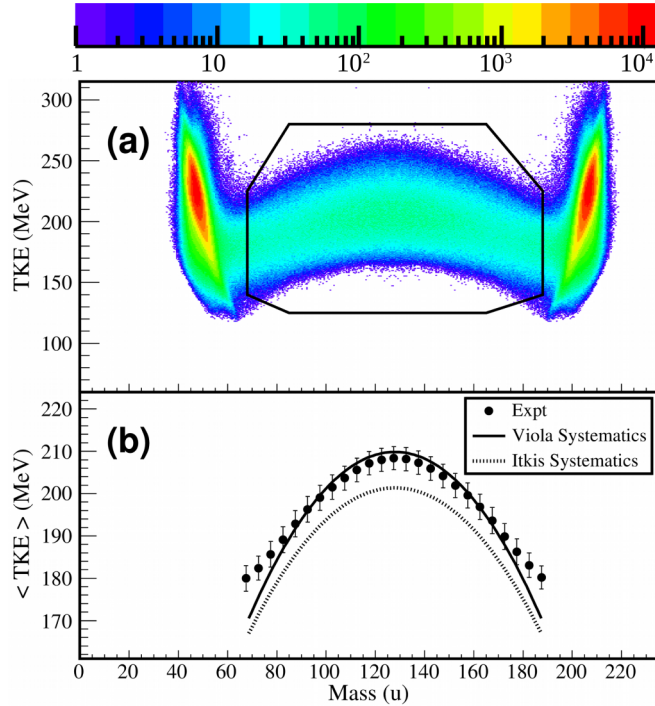
FIG. 4. (a) The scatter plot of mass and TKE of fission fragments and color palette (on top) represents the counts and (b) the variation of $\langle \text{TKE} \rangle$ with the fragment mass for the gated region (black gate shown in the upper panel) for the $^{48}\text{Ti} + {}^{208}\text{Pb}$ reaction.

detector at zero degree to the fission detector and perpendicular to the fission detector are around 40 000 and 6000 respectively.

The angles θ and ϕ of the emitted fragments are obtained from their calibrated position spectra. These emission angles and TOF information of the fission fragments are deployed to derive their velocity vectors. Furthermore, the masses and kinetic energies of the fission fragments are determined from the extracted velocities and angles using the binary kinematics, followed by an iterative procedure as described in Ref. [18]. The center-of-mass total kinetic energy (TKE) of the fission fragments are deduced from the masses and velocities of the fission fragments. The scatter plot of mass and TKE shown in Fig. 4(a), comprises the FF and QF events lying in intermediate region between the strong peaks arising from the elastic process, quasielastic process, and DIC. Figure 4(b) shows the variation of average TKE ($\langle \text{TKE} \rangle$) with the fragment mass corresponding to the intermediate region [black gate drawn in Fig. 4(a)] and the comparison with the Viola systematics [27] (solid line) and the Itkis systematics [28] (dotted line). This comparison assures the good agreement with the liquid drop model of fission by indicating the parabolic dependence of $\langle \text{TKE} \rangle$ on the fragment masses.

The MED of the fission fragments indicates the overlap of the FF and QF events in the intermediate mass region. Therefore, to separate out the contribution of FF and QF events, neutron multiplicity measurements are carried out in correlation with the binary fragments. The dependence of neutron multiplicity on the mass and TKE of the fission fragments is presented in the following subsections.

A. Variation of neutron multiplicity with mass

To analyze the dependence of neutron multiplicity on the mass of the fission fragments, the MED is divided into three mass sections, viz., projectile-like fragments (PLF) ($38 \leqslant A_{\text{FF}} \leqslant 68$) and asymmetric ($68 \leqslant A_{\text{FF}} \leqslant 108$) and symmetric ($A_{\text{FF}} = \frac{A_{\text{CN}}}{2} \pm 20$) mass regions. Here, A_{FF} and A_{CN} specify the mass of the fission fragments and CN respectively. Furthermore, to minimize the angular uncertainty stemming from the large effective area of MWPC, it is segmented into four identical slices of dimension 30×50 mm. The slicing of MWPC and the width of mass window are decided in order to allow sufficient statistics in all the 388 neutron energy spectra corresponding to each mass cut. The neutron energy spectra are then corrected for the energy-dependent neutron detection efficiency obtained using the FLUKA code. The neutron energy spectra are assumed to receive contributions from the three sources, namely, the emission from the composite nucleus (prescission) and the emission from one of the fission fragments (F1) and its complementary fragment (F2) (postscission). The neutrons emitted from these moving sources are assumed to be distributed isotropically in their respective center-of-mass frames. The theoretical Watt expression [29] for the neutron energy spectrum summed over the three aforementioned moving sources can be written as

$$\frac{d^2 M_n}{dE_n d\Omega_n} = \sum_{i=1}^{3} \frac{M_n^i \sqrt{E_n}}{2(\pi T_i)^{3/2}} \exp\left[-\frac{E_n - 2\sqrt{\epsilon_i E_n} \cos \Psi_i + \epsilon_i}{T_i} \right],$$

$$(2)$$

where M_n^i, ϵ_i, and T_i are the multiplicity, energy per nucleon, and temperature of the ith neutron source respectively. E_n is the measured laboratory energy of the neutrons. Ψ_i is the relative angle between the direction of neutron (θ_n, ϕ_n) and the ith emitting source. The experimentally measured folding angles and energies of F1 and F2 corresponding to each mass cut are consistent with the Viola systematics and kinematical calculations. So, the experimentally measured values of ϵ_i and folding angles for the F1 and F2 are used in the fitting procedure.

The prescission neutrons can be separated from the postscission ones on the basis of their different fission-neutron angular correlations. To extract prescission (M_n^{pre}) and postscission (M_n^{F1}, M_n^{F2}) neutron multiplicities, all the 388 double differential neutron multiplicity spectra corresponding to each mass cut are simultaneously fitted using Eq. (2) with the multiple-source least-square fitting method followed by the χ^2 minimization procedure. During this fitting procedure, three neutron multiplicities (M_n^{pre}, M_n^{F1}, M_n^{F2}) and their corresponding temperatures (T_{pre}, T_{F1}, T_{F2}) are treated as free parameters. The angular acceptance of both the fission and neutron detectors are taken into consideration during the fitting procedure. The minimum value of χ^2/(number of degrees of freedom) lies in between 1.7 and 2.4 for all the three mass cuts. This simultaneous fitting is also performed by fixing the $T_{\text{pre}} = \sqrt{\frac{E^*}{a}}$, where E^* is the excitation energy of CN and a is the nuclear level density parameter which is taken to be $A_{\text{CN}}/10$ MeV^{-1}. The values of neutron multiplicities thus obtained are found to lie in the close proximity with the ones
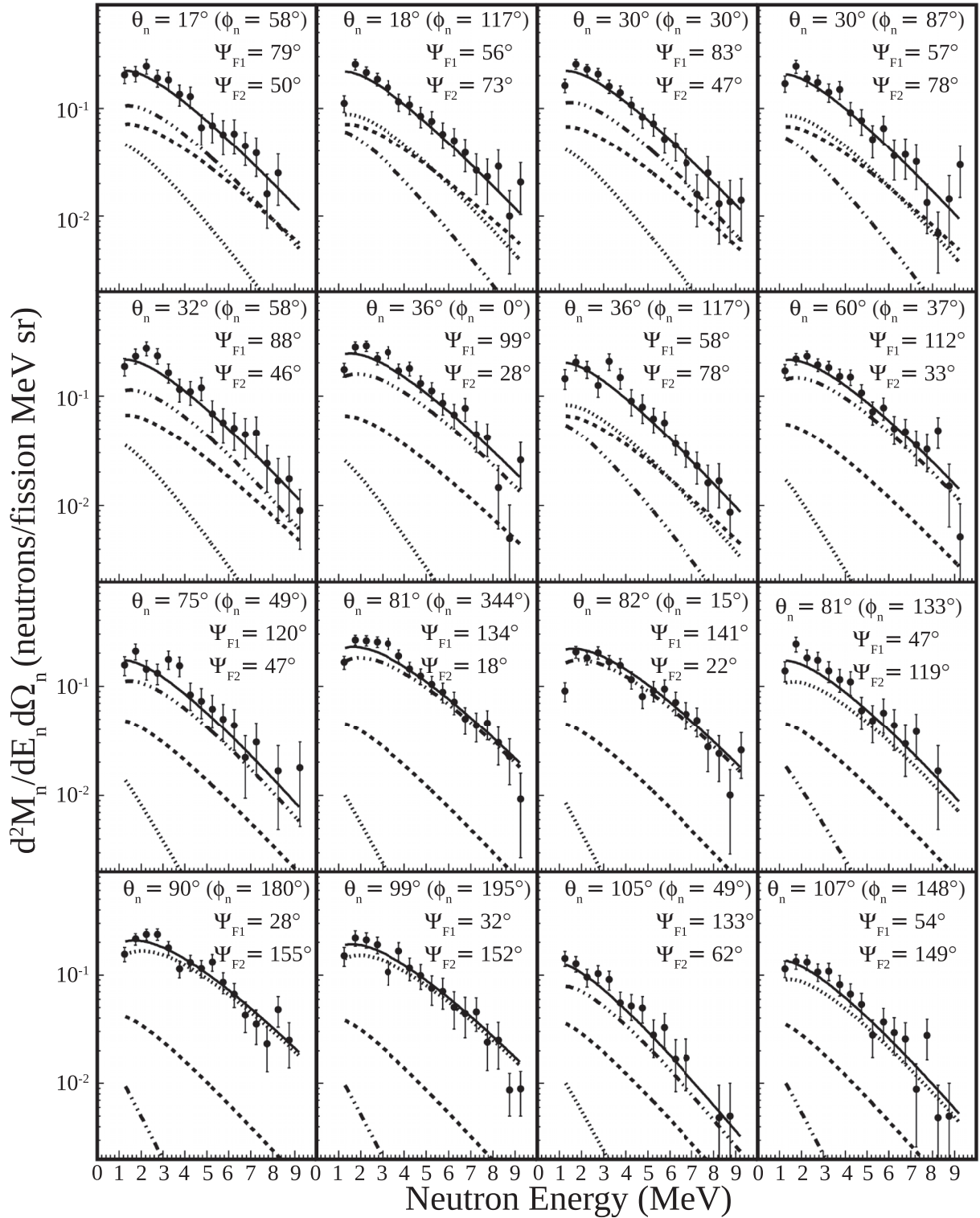
FIG. 5. Double differential neutron multiplicity spectra for the ^{48}Ti + ^{208}Pb reaction at an excitation energy of 57.4 MeV for the different neutron detectors corresponding to the symmetric mass cut ($A_{FF} = \frac{A_{CN}}{2} \pm 20$). The fits for the prescission (dashed lines) and postscission contributions from the fragment F1 (dotted lines) and those from the fragment F2 (dash-dotted lines) are indicated. The solid lines correspond to the total neutron contribution. The relative angles between the fragments and the detected neutron are also quoted.
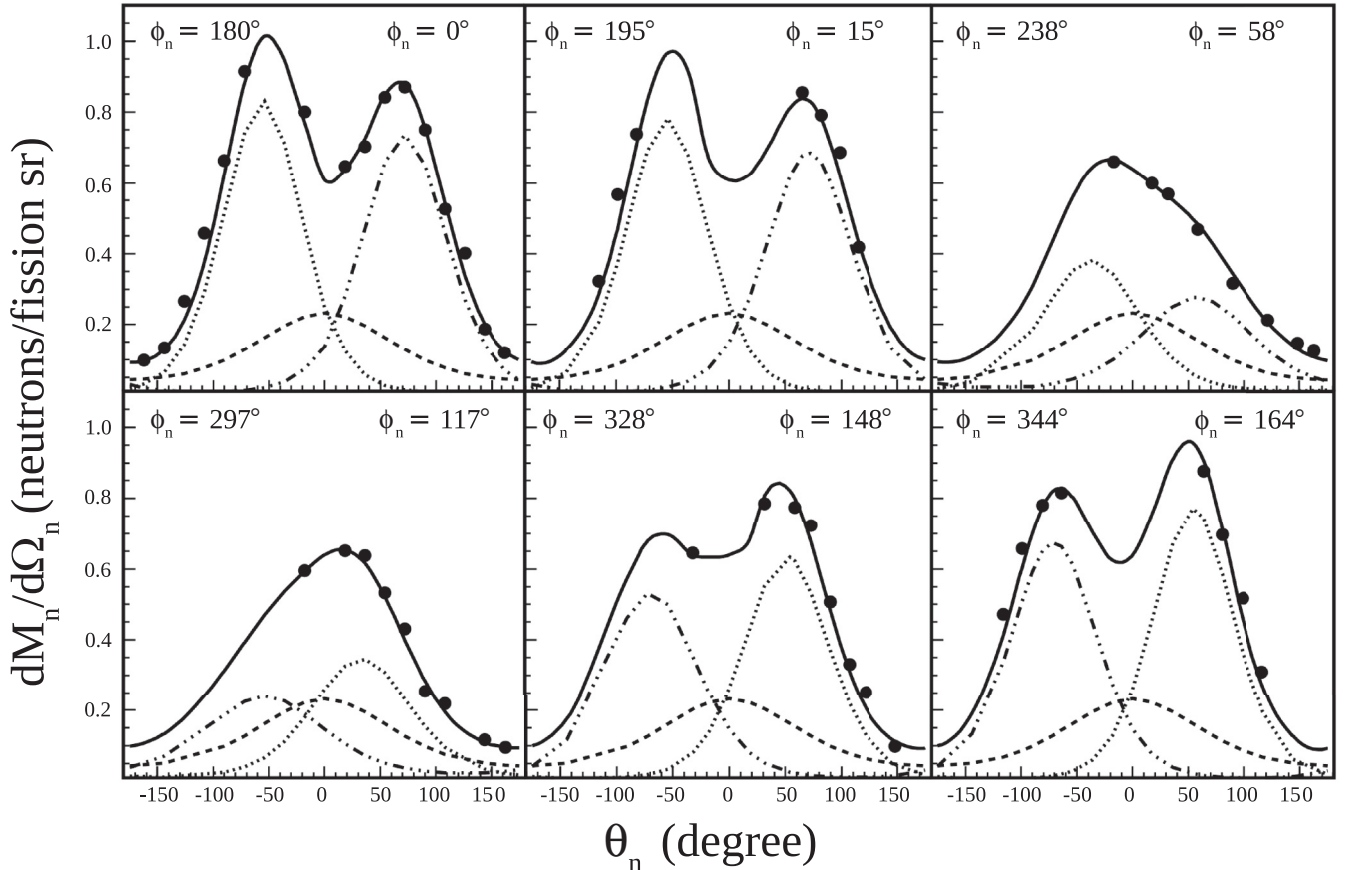
FIG. 6. The multiple-source fitting (solid lines) to the experimental neutron θ_n (in the laboratory frame) distributions (solid circles) for the ^{48}Ti + ^{208}Pb reaction for the different ϕ_n corresponding to the symmetric mass cut. The dashed lines correspond to the prescission contribution while the dotted and dash-dotted lines indicate the individual postscission contributions from fragments F1 and F2 respectively.

deduced while treating the T_{pre} as a free parameter. Figure 5 shows the fitted double differential neutron multiplicity spectra at different angles for the symmetric mass cut, which clearly indicates the strong dependence of the contributions from different neutron sources with Ψ_i. This dependence primarily arises due to the kinematic focusing of emitted neutrons in the direction of accelerated fragments. The differential neutron yield is obtained by integrating the double differential neutron multiplicity spectra over neutron energy from 0 to 6 MeV. Figure 6 shows the angular distributions of neutrons both in and out of the reaction plane corresponding to the symmetric mass cut. The experimental outcomes are also compared with the total contribution from all the neutron sources derived using the moving source fitting procedure. The individual contribution from each neutron source is also revealed in Fig. 6, where the contribution from the CN is a Gaussian centered around 0° while for the neutron contributions from F1 and F2, the Gaussian distributions are peaking around the centers of the respective MWPCs. Hence, these distributions also assert the onset of kinematic focusing as observed in Fig. 5.

The obtained values of M_n^{pre}, M_n^{post}, M_n^{total}, T_{pre}, T_{F1}, and T_{F2} for the different mass cuts are listed in Table I. Here, $M_n^{\text{post}} = M_n^{\text{F1}} + M_n^{\text{F2}}$ is the total postscission neutron multiplicity component and $M_n^{\text{total}} = M_n^{\text{pre}} + M_n^{\text{post}}$ is the total neutron multiplicity. From Table I, it is observed that M_n^{total}

increases from the value 0.44 ± 0.02 to 8.25 ± 0.10 while moving from PLF to symmetric mass split. In the same manner, M_n^{pre} is also found to increase from PLF ($M_n^{\text{pre}} = 0.15 \pm 0.01$) to symmetric ($M_n^{\text{pre}} = 2.23 \pm 0.07$) mass split which could be justified qualitatively based on the expected enhancement of the available excitation energy with transition from PLF to symmetric mass split. In our recently published work, the substantial presence of QF ($\sim$35%) events in the asymmetric part of the reaction product mass distribution of the ^{48}Ti + ^{208}Pb system is estimated using the theoretical calculations of dinuclear systems [18]. Hence, the enhancement in M_n^{pre} while transition from asymmetric ($M_n^{\text{pre}} = 1.66 \pm 0.07$) to symmetric ($M_n^{\text{pre}} = 2.23 \pm 0.07$) mass region might be due to the different timescales of the FF and QF processes. The observed neutron multiplicities for three mass splits are compatible with the recent results reported for the nearby system ^{50}Ti + ^{208}Pb [30]. However, the uncertainties on our results are very small as compared to those reported in earlier similar measurements, which is the advantage of using the multidetector NAND array for such measurements.

The decay of the intermediate composite system could be investigated using the total available decay energy for a particular exit channel and the energy cost for the neutron emission. So, to check the consistency of the experimental data, the measured neutron multiplicities corresponding to

TABLE I. Neutron multiplicity and temperature values for the ^{48}Ti + ^{208}Pb system corresponding to different fission fragment mass splits.

Mass cuts	M_n^{pre}	M_n^{post}	M_n^{total}	T_{pre} (MeV)	T_{F1} (T_{F2}) (MeV)
PLF mass cut ($38 \leqslant A_{\text{FF}} \leqslant 68$)	0.15 ± 0.01	0.29 ± 0.02	0.44 ± 0.02	1.55 ± 0.15	1.17 ± 0.14 (1.23 ± 0.13)
Asymmetric mass cut ($68 \leqslant A_{\text{FF}} \leqslant 108$)	1.66 ± 0.07	5.32 ± 0.05	6.98 ± 0.09	1.78 ± 0.04	1.33 ± 0.02 (1.39 ± 0.01)
Symmetric mass cut ($A_{\text{FF}} = \frac{A_{\text{CN}}}{2} \pm 20$)	2.23 ± 0.07	6.02 ± 0.07	8.25 ± 0.10	1.79 ± 0.03	1.39 ± 0.01 (1.39 ± 0.01)

symmetric and asymmetric mass splits are compared with the values predicted using the energy balance equation [31]. Based on this formulation, two different methods can be followed to extract the total available decay energy. In the first method, the total available decay energy [$E_x(f)$] for a particular exit channel is expressed in terms of the initial excitation energy (E^*) of the CN as given in the following equation:

$$E_x(f) = E^* + Q_{ff}(f) - \langle TKE \rangle(f), \quad (3)$$

where Q_{ff} is the average Q value of the CN fission. In the second method, the experimentally deduced M_n^{total} is used to calculate $E_x(f)$ as given in the following equation, assuming that the total available decay energy is carried away by γ-ray and neutron emission:

$$E_x(f) = E_\gamma(f) + \sum_{i=1}^{M_n^{\text{total}}} \left(B_n + E_n^i \right), \quad (4)$$

where E_γ is the total γ-ray energy, B_n is the average binding energy of neutron, and E_n^i is the kinetic energy of the ith emitted neutron. The deduced value of $E_x(f)$ using the aforementioned methods are consistent within ± 5 MeV, which indicates that our experimentally extracted values of M_n^{total} corresponding to symmetric and asymmetric mass splits are in agreement with the available E^* of the CN.

For both the symmetric and asymmetric mass splits, the available excitation energy of nuclei at the scission point (E_{sc}^*) and the excitation energy of the fission fragments (E_{ff}^*) are also estimated using the formulation described elsewhere [15,31]. The excitation energy of the individual fission fragments at scission point ($E_{sc}^{*\text{ind}}$) is then obtained by assuming that E_{sc}^* is shared between the fission fragments F1 and F2 in proportion to their respective masses and is given as

$$E_{sc}^{*\text{ind}} = \frac{A_{\text{FF}}}{A_{\text{CN}}} E_{sc}^*. \quad (5)$$

Figure 7 illustrates the variation of the excitation energy of fission fragments with the mass of the fission fragments, where the solid curve represents the values of $E_{sc}^{*\text{ind}}$ derived using Eq. (5) and solid circles indicate the actual E_{ff}^*. The values of E_{ff}^* and $E_{sc}^{*\text{ind}}$ are consistent within error bars as shown in Fig. 7, which implies that the total available excitation energy of the fission fragments is divided in proportion to their masses. Hence, one can assert that the complete thermalization

of the fissioning nucleus occurs at any mass ratio of the fission fragment.

From the theoretical dinuclear system calculations for mass distribution of this system, QF contributions are found to be negligible in the symmetric mass region [18]. From an extrapolation of the measured total neutron multiplicity for the symmetric mass region to zero E^*, the average number of prompt neutrons (M_n^{sf}) emitted in the spontaneous fission of ^{256}Rf are deduced from the derived average energy cost for the emitted neutrons. The extracted value of M_n^{sf} for ^{256}Rf is 4.4 ± 1.0, which is compatible with the ones reported for ^{258,260}Rf isotopes [30,32]. This value is also consistent with the systematics of spontaneous fission of superheavy nuclei [16,33].

B. Variation of neutron multiplicity with TKE

In order to further investigate the fission dynamics of ^{256}Rf nucleus, the dependence of neutron multiplicities on the TKE of the fission fragments is checked by performing the multiple-source least square fitting method for the different TKE cuts corresponding to the intermediate mass region. It is observed that the straight horizontal cuts in TKE result in different mass distributions for each TKE cut as discussed in Ref. [18]. In order to ensure the approximately same mass distribution corresponding to each cut, Hinde *et al.* have suggested gating on the defined related parameter, RTKE, the ratio of the experimentally extracted TKE to that determined from the Viola systematics with the inclusion of dependence
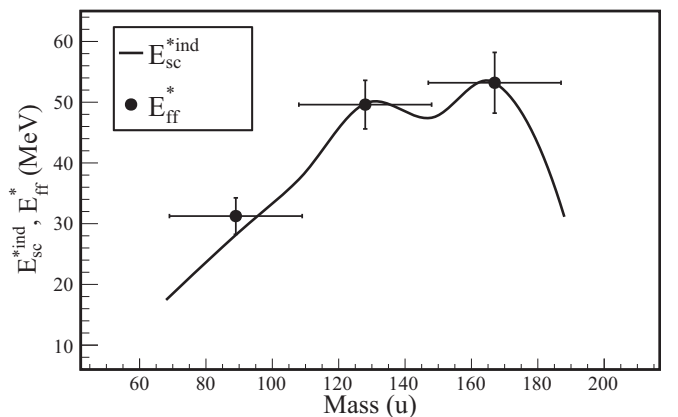

FIG. 7. Variation of excitation energy of the fission fragments as a function of their mass for the ^{48}Ti + ^{208}Pb reaction (see text).
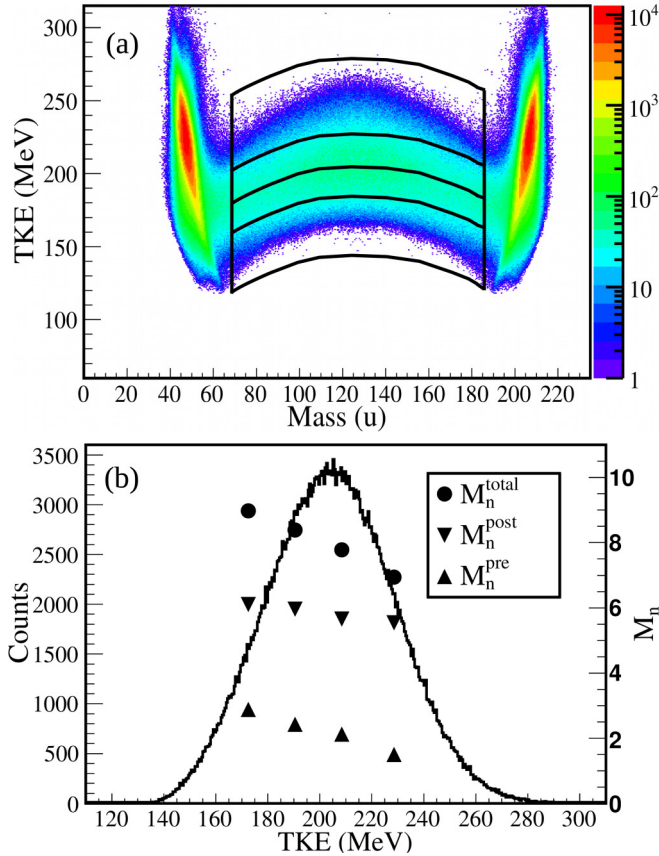
FIG. 8. (a) The four RTKE cuts applied on the MED matrix of the fission fragments as explained in the text. (b) Total projection of TKE in the considered mass window together with the extracted values of prescission (solid upward-pointing triangles), postscission (solid downward-pointing triangles), and total (solid circles) neutron multiplicities plotted at the mean TKE values corresponding to the four RTKE cuts shown in the top panel.

of mass asymmetry [34]. In the upper panel of Fig. 8, the appearance of these linear cuts in RTKE applied to the MED matrix of the fission fragments is indicated. The selection of the number of RTKE cuts and their span is done in such a way that each neutron spectra have sufficient statistics to carry out the multiple-source fitting corresponding to each RTKE cut. The kinematic effects and recoil effects due to the postscission neutrons are taken into account in this fitting procedure. The lower panel of Fig. 8 shows the projection of TKE in the considered intermediate mass window, along with the extracted values of M_n^{pre}, M_n^{post}, and M_n^{total} at the respective mean TKE values corresponding to the four considered RTKE cuts.

Here, M_n^{pre} is found to decrease with increase in TKE. This trend clearly indicates the presence of QF processes in this heavy system. As in the case of QF, the neutron lifetime can be significantly shorter than the acceleration time of the fragments so that the hypothesis made for the fitting procedure that the neutrons are emitted from fully accelerated fragments is no longer valid. Consequently, neutrons emitted after scission but before the fragments have reached their asymptotic velocities are misidentified as prescission neutrons in the multiple-source

fitting. The number of these prescission neutrons sensitively depends on TKE. Since a high TKE means low thermal energy, and it thereby results in long neutron lifetimes and a small probability of neutron emission during acceleration. Conversely, a low TKE corresponds to high thermal energy and results in more acceleration neutrons.

IV. STATISTICAL MODEL CALCULATIONS

The experimentally extracted M_n^{pre} and M_n^{post} are next compared with the statistical model predictions for the ^{48}Ti $+ \, ^{208}$Pb system. The statistical model calculations are based on the assumption that the whole of the incident flux leads to the CN formation [35]. The CN can decay into either of the two major products, namely an evaporation residue or the fission fragments along with the emission of light particles such as neutrons, protons, α particles, and γ rays. Assuming the symmetric fission, the fission width Γ_{BW} is obtained from the transition-state model of fission given by Bohr and Wheeler [36], while the particle and γ emission widths are obtained from the Weisskopf formula as given in Ref. [37]. A phase-space factor due to the collective motion in the ground state is included in Γ_{BW} [38].

The fission barrier in the present calculations is obtained by including shell correction in the liquid-drop nuclear mass [39]. The shell correction term δ is given as the difference between the experimental and the liquid-drop model (LDM) masses ($\delta = M_{\text{exp}} - M_{\text{LDM}}$). The angular momentum dependent fission barrier is then given as

$$B_f(l) = B_f^{\text{LDM}}(l) - (\delta_g - \delta_s), \qquad (6)$$

where $B_f^{\text{LDM}}(l)$ is the angular-momentum-dependent LDM fission barrier [40], and δ_g and δ_s are the shell correction energies for the ground-state and saddle configurations respectively. For δ_g and δ_s, we use the prescription given in Ref. [41] for deformation dependence of shell correction which gives a very small value of shell correction at large deformations and full shell correction at zero deformation.

Shell effect is also included in the nuclear level density which is used to calculate various decay widths of the CN. To this end, we use the level density parameter from the work of Ignatyuk *et al.* [42], which includes shell effects at low excitation energies and goes over to its asymptotic form at high excitation energies. The shape-dependent asymptotic level density parameter is taken from Ref. [43].

In the statistical model of CN decay, fission occurs when the CN crosses the saddle point. The number of neutrons emitted by the CN during its progression from the saddle to the scission configuration contributes to M_n^{pre} and is calculated using the saddle-to-scission transit time interval [44,45] given as

$$\tau_{ss}^o = \frac{2}{\omega_s} R \left[\left(\frac{\Delta V}{T} \right)^{\frac{1}{2}} \right], \qquad (7)$$

where

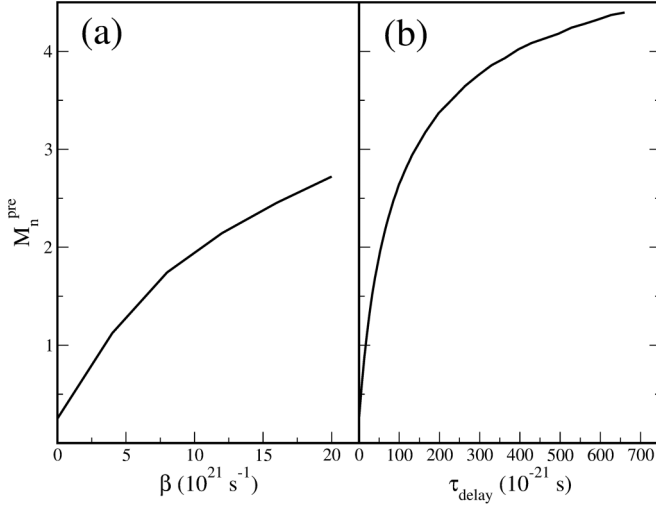$$R(z) = \int_0^z \exp(y^2) dy \int_y^\infty \exp(-x^2) dx$$

FIG. 9. Variation of the prescission neutron multiplicity (M_n^{pre}) with (a) the reduced dissipation coefficient (β) and (b) delay time (τ_{delay}) for the ^{48}Ti + ^{208}Pb reaction at an excitation energy of 57.4 MeV.

and ΔV is the potential difference between the saddle and the scission points. ω_s is the frequency of a harmonic oscillator potential which approximates the nuclear potential near the saddle configuration and T is the nuclear temperature.

The calculated value of the prescission neutron multiplicity M_n^{pre} for the reaction ^{48}Ti + ^{208}Pb at a CN excitation energy of 57.4 MeV ($E_{\text{lab}} = 273.1$ MeV) is 0.25 including a saddle-to-scission contribution of 0.21. This clearly indicates that a longer fission timescale is required in order to emit the experimentally observed number of prescission neutrons. It is also indicated that most of the prescission neutrons are emitted in the saddle-to-scission stage due to very high fissility of the CN ^{256}Rf.

The above observations immediately suggest that a fission hindrance is required to reproduce the prescission neutron multiplicity. In a dissipative dynamical model of fission, a reduction in fission width can be obtained from the Kramers modified fission width given as [20]

$$\Gamma_K = \Gamma_{\text{BW}} \left[\sqrt{1 + \left(\frac{\beta}{2\omega_s}\right)^2} - \frac{\beta}{2\omega_s} \right], \qquad (8)$$

where Γ_{BW} is the Bohr-Wheeler fission width and β is the reduced dissipation coefficient (ratio of the dissipation coefficient to inertia). Introduction of dissipation also changes the saddle-to-scission time interval and is given as [44]

$$\tau_{ss} = \tau_{ss}^o \left[\sqrt{1 + \left(\frac{\beta}{2\omega_s}\right)^2} + \frac{\beta}{2\omega_s} \right]. \qquad (9)$$

Statistical model calculations are performed for the different values of β and the variation of M_n^{pre} with β is given in Fig. 9(a). The major contribution to M_n^{pre} values calculated with β also comes during the saddle-to-scission transition of the CN, e.g., M_n^{pre} obtained with $\beta = 10 \times 10^{21}$ s^{-1} is 1.94 including the saddle-to-scission contribution of 1.65. We find that the

experimental value of M_n^{pre} (2.23 $\pm$ 0.07) for the symmetric mass cut can be reproduced by the β value of (13.0 $\pm$ 1.0) $\times$ 10^{21} s^{-1}. The strength of the dissipation thus found is close to the values used in earlier works [46,47]. By following the decay of the fission fragments, we also obtain the value of M_n^{post} and the resulting M_n^{total} value is 8.60, which compares favorably with the experimental value of (8.25 $\pm$ 0.10) obtained for the symmetric mass cut.

In order to get a direct estimate of time delay required for emission of the experimentally observed number of prescission neutrons, we perform another set of calculations where a delay time (τ_{delay}) is introduced in the saddle-to-scission stage of fission. The total saddle-to-scission transition time is then given as ($\tau_{ss}^o + \tau_{\text{delay}}$). No dissipation is considered in this calculation. The variation of M_n^{pre} with τ_{delay} is shown in Fig. 9(b). It is observed that a fission delay of $(67.3^{+5.3}_{-3.9}) \times$ 10^{-21} s corresponds to the experimentally observed value of M_n^{pre} (2.23 $\pm$ 0.07) for the symmetric mass cut. A comparable mean fission delay time of 45×10^{-21} s was observed in an earlier work [30] to account for the M_n^{pre} in fission of ^{258}Rf at an excitation energy of 64 MeV. A fission delay of $(50^{+120}_{-30}) \times$ 10^{-21} s in decay of ^{260}Rf at an excitation energy of 180 MeV was also observed in Ref. [32]. However, the uncertainties associated with the delay times reported in the above referred works are much larger than that obtained here due to the better accuracy achieved in experimental determination of neutron multiplicities in the present work.

The value of M_n^{pre} for the asymmetric mass cut is determined as (1.66 $\pm$ 0.07) in the present experiment. This value is well resolved from the multiplicity (2.23 $\pm$ 0.07) for symmetric mass cut in comparison to the overlapping multiplicities of symmetric and asymmetric mass cuts reported in a previous work [30]. As discussed previously, a substantial presence of QF events in the asymmetric part of the reaction product mass distribution of the present system is predicted from the dinuclear system calculations. The present statistical model results, however, should not be directly used to extract the delay time for the asymmetric fission without a word of caution. This mainly concerns the magnitude of the neutron width used to calculate the number of evaporated neutrons in a given time interval. The neutron width depends sensitively on the neutron separation energy of the CN, which in turn can depend on the compound nuclear deformation. For symmetric fission, however, it is shown that the neutron separation energy does not change appreciably with compound nuclear deformation [48]. We therefore approximate the neutron width required to calculate the neutron multiplicity during the saddle-to-scission transition for symmetric fission with the neutron width as obtained for the spherical nucleus. However, this approximation may lose its validity for asymmetrical shapes of the CN. Further, the calculated values of M_n^{pre} correspond to the CN excitation energy available for the symmetric fission while the excitation energy for asymmetric fission should be smaller. We therefore refrain from associating the time delay of 28×10^{-21} s which can account for the value of 1.66 for M_n^{pre} [from Fig. 9(b)] with the timescale of asymmetric fission. This clearly points to the need for a statistical model analysis of asymmetric fission in order to interpret the neutron multiplicity and to find signature of the QF processes.

V. SUMMARY AND CONCLUSIONS

The presence of QF processes has been confirmed through the MD, MED, and MAD analyses of the fission fragments produced in the ^{48}Ti $+$ ^{208}Pb reaction populating near superheavy CN ^{256}Rf at an excitation energy of 57.4 MeV. In the present paper, the dependence of neutron multiplicities on the fission observables (mass and TKE) has been investigated to further understand the fission dynamics of ^{256}Rf. Besides the neutron multiplicity measurements, the experimental neutron angular distributions have been measured which indicate the kinematic focusing of emitted neutrons in the direction of accelerated fragments. The analysis of mass-split and TKE dependence of M_n^{pre} also reveals non-negligible contributions of QF processes along with the FF processes. M_n^{pre} is observed to increase while moving from asymmetric to symmetric mass region, which is due to the different timescales of the FF and QF processes. M_n^{pre} is found to increase with decreasing TKE, a trend which the recoil and kinematics corrections can only reinforce. This trend is mainly an artifact of neutron emission during acceleration of the fragments, which are identified as the prescission component in the fits. Increasing thermal energy by reducing the TKE results in even shorter lifetimes and thereby increases the neutron emission during acceleration. Additionally, the dependence of neutron multiplicities on mass split has been compared with the outcomes based on the energy balance equation and are found to be consistent with each other within a systematic uncertainty of $\leqslant 5\%$. Statistical model calculations show that most of the prescission neutrons are emitted during the saddle-to-scission transition of the compound nuclei for the symmetric fission. The strength of the reduced dissipation coefficient to account for the experimentally measured multiplicity of prescission neutrons is found to be $(13.0 \pm 1.0) \times 10^{21}$ s^{-1}. Alternately, the experimental prescission neutron multiplicity for the symmetric mass cut is also reproduced by introducing a delay time of $(67.3^{+5.3}_{-3.9}) \times 10^{-21}$ s in the saddle-to-scission stage of fission. No attempt is, however, made in the present work to reproduce the prescission neutron multiplicities obtained with asymmetric mass cut since the statistical model analysis is limited to symmetric fission. The average neutron multiplicity (M_n^{sf}) from the spontaneous fission of ^{256}Rf is also extracted from the measured total neutron multiplicity for the symmetric mass split and found to be 4.4 ± 1.0, which is compatible with the recently published data for ^{258,260}Rf isotopes and the previously reported findings for the superheavy nuclei.

In future, we plan to extend these measurements over wider range of excitation energies in order to estimate the contributions of QF and FF processes quantitatively. It is also planned to study the role of entrance channel effects in the reaction dynamics to form superheavy nuclei.

[1] A. Sobiczewski, F. A. Gareev, and B. N. Kalinkin, Phys. Lett. **22**, 500 (1966).

[2] S. Hofmann and G. Münzenberg, Rev. Mod. Phys. **72**, 733 (2000).

[3] K. Morita, K. Morimoto, D. Kaji, T. Akiyama, S.-i. Goto, H. Haba, E. Ideguchi, R. Kanungo, K. Katori, H. Koura *et al.*, J. Phys. Soc. Jpn. **73**, 2593 (2004).

[4] Y. T. Oganessian, Nucl. Phys. A **787**, 343c (2007).

[5] R. Bock, Y. T. Chu, M. Dakowski, A. Gobbi, E. Grosse, A. Olmi, H. Sann, D. Schwalm, U. Lynen, W. Müller *et al.*, Nucl. Phys. A **388**, 334 (1982).

[6] J. Tõke, R. Bock, G. X. Dai, A. Gobbi, S. Gralla, K. D. Hildenbrand, J. Kuzminski, W. F. J. Müller, A. Olmi, H. Stelzer *et al.*, Nucl. Phys. A **440**, 327 (1985).

[7] B. B. Back, R. R. Betts, J. E. Gindler, B. D. Wilkins, S. Saini, M. B. Tsang, C. K. Gelbke, W. G. Lynch, M. A. McMahan, and P. A. Baisden, Phys. Rev. C **32**, 195 (1985).

[8] V. S. Ramamurthy and S. S. Kapoor, Phys. Rev. Lett. **54**, 178 (1985).

[9] W. U. Schröder and J. R. Huizenga, in *Damped Nuclear Reactions, Treatise on Heavy-ion Science*, edited by D. A. Bromley (Plenum Press, New York, 1984), Vol. 2, p. 115.

[10] R. Rafiei, R. G. Thomas, D. J. Hinde, M. Dasgupta, C. R. Morton, L. R. Gasques, M. L. Brown, and M. D. Rodriguez, Phys. Rev. C **77**, 024606 (2008).

[11] C. Simenel, D. J. Hinde, R. du Rietz, M. Dasgupta, M. Evers, C. J. Lin, D. H. Luong, and A. Wakhle, Phys. Lett. B **710**, 607 (2012).

[12] S. Kailas and K. Mahata, Pramana J. Phys. **83**, 851 (2014).

[13] E. M. Kozulin, G. N. Knyazheva, I. M. Itkis, M. G. Itkis, A. A. Bogachev, L. Krupa, T. A. Loktev, S. V. Smirnov, V. I. Zagrebaev, J. Äystö *et al.*, Phys. Lett. B **686**, 227 (2010).

[14] W. Q. Shen, J. Albinski, A. Gobbi, S. Gralla, K. D. Hildenbrand, N. Herrmann, J. Kuzminski, W. F. J. Müller, H. Stelzer, J. Toke, B. B. Back, S. Bjrnholm, and S. P. Srensen, Phys. Rev. C **36**, 115 (1987).

[15] M. G. Itkis, J. Äystö, S. Beghini, A. A. Bogachev, L. Corradi, O. Dorvaux, A. Gadea, G. Giardina, F. Hanappe, I. M. Itkis *et al.*, Nucl. Phys. A **734**, 136 (2004).

[16] P. K. Sahu, R. G. Thomas, A. Saxena, R. K. Choudhury, S. S. Kapoor, L. M. Pant, M. Barbui, M. Cinausero, G. Prete, V. Rizzi *et al.*, Phys. Rev. C **72**, 034604 (2005).

[17] R. S. Naik, W. Loveland, P. H. Sprunger, A. M. Vinodkumar, D. Peterson, C. L. Jiang, S. Zhu, X. Tang, E. F. Moore, and P. Chowdhury, Phys. Rev. C **76**, 054604 (2007).

[18] M. Thakur, B. R. Behera, R. Mahajan, N. Saneesh, G. Kaur, P. Sharma, R. Dubey, K. Kapoor, A. Yadav, N. Kumar *et al.*, Eur. Phys. J. A **53**, 133 (2017).

[19] P. Sugathan, A. Jhingan, K. S. Golda, T. Varughese, S. Venkataramanan, N. Saneesh, V. V. Satyanarayana, S. K. Suman, J. Antony, R. Shanti *et al.*, Pramana **83**, 807 (2014).

[20] H. A. Kramers, Physica (Amsterdam, Neth.) **7**, 284 (1940).

[21] M. Thakur, R. Dubey, S. R. Abhilash, B. R. Behera, B. P. Mohanty, D. Kabiraj, S. Ojha, and H. Duggal, MethodsX **3**, 542 (2016).

[22] A. Jhingan, Pramana J. Phys. **85**, 483 (2015).

[23] N. Saneesh, M. Thakur, R. Mahajan, G. Kaur, R. Dubey, S. Venkataramanan, A. Jhingan, and P. Sugathan, Proc. DAE Symp. Nucl. Phys. **58**, 986 (2013).

[24] S. Venkataramanan, A. Gupta, K. S. Golda, H. Singh, R. Kumar, R. P. Singh, and R. K. Bhowmik, Nucl. Instrum. Methods Phys. Res., Sect. A **596**, 248 (2008).

[25] *Proceedings of an Advisory Group Meeting on Properties of Neutron Sources*, IAEA-TECDOC-410, International Atomic Energy Agency (Vienna, Austria, 1987).

[26] A. Ferrari, P. R. Sala, A. Fasso, and J. Ranft, FLUKA: A multiparticle transport code, CERN-2005-10, INFN/TC_05/11, SLAC-R-773, 2005.

[27] V. E. Viola, K. Kwiatkowski, and M. Walker, Phys. Rev. C **31**, 1550 (1985).

[28] M. G. Itkis and A. Y. Rusanov, Phys. Part. Nuclei **29**, 160 (1998).

[29] D. Hilscher, J. R. Birkelund, A. D. Hoover, W. U. Schröder, W. W. Wilcke, J. R. Huizenga, A. C. Mignerey, K. L. Wolf, H. F. Breuer, and V. E. Viola, Phys. Rev. C **20**, 576 (1979).

[30] S. Appannababu, M. Cinausero, T. Marchi, F. Gramegna, G. Prete, J. Bermudez, D. Fabris, G. Collazuol, A. Saxena, B. K. Nayak *et al.*, Phys. Rev. C **94**, 044618 (2016).

[31] D. J. Hinde, R. J. Charity, G. S. Foote, J. R. Leigh, J. O. Newton, S. Ogaza, and A. Chattejee, Nucl. Phys. A **452**, 550 (1986).

[32] A. Saxena, D. Fabris, G. Prete, D. V. Shetty, G. Viesti, B. K. Nayak, D. C. Biswas, R. K. Choudhury, S. S. Kapoor, M. Lunardon *et al.*, Nucl. Phys. A **730**, 299 (2004).

[33] R. G. Thomas, A. Saxena, P. K. Sahu, R. K. Choudhury, I. M. Govil, S. Kailas, S. S. Kapoor, M. Barbui, M. Cinausero, G. Prete, V. Rizzi, D. Fabris, M. Lunardon, S. Moretto, G.Viesti, G. Nebbia, S. Pesente, B. Dalena, G. D'Erasmo, E. M. Fiore, M. Palomba, A. Pantaleo, V. Paticchio, G. Simonetti, N. Gelli, and F. Lucarelli, Phys. Rev. C **75**, 024604 (2007).

[34] D. J. Hinde, D. Hilscher, H. Rossner, B. Gebauer, M. Lehmann, and M. Wilpert, Phys. Rev. C **45**, 1229 (1992).

[35] J. Sadhukhan and S. Pal, Phys. Rev. C **78**, 011603(R) (2008); **79**, 019901(E) (2009).

[36] N. Bohr and J. A. Wheeler, Phys. Rev. **56**, 426 (1939).

[37] P. Fröbrich and I. I. Gontchar, Phys. Rep. **292**, 131 (1998).

[38] V. M. Strutinsky, Phys. Lett. B **47**, 121 (1973).

[39] K. Mahata, S. Kailas, and S. S. Kapoor, Phys. Rev. C **92**, 034602 (2015).

[40] A. J. Sierk, Phys. Rev. C **33**, 2039 (1986).

[41] W. D. Myers and W. J. Swiatecki, Nucl. Phys. **81**, 1 (1966).

[42] A. V. Ignatyuk, G. M. Smirenkin, and A. Tishin, Sov. J. Nucl. Phys. **21**, 255 (1975).

[43] W. Reisdorf, Z. Phys. A **300**, 227 (1981).

[44] H. Hofmann and J. R. Nix, Phys. Lett. B **122**, 117 (1983).

[45] P. Grangé, S. Hassani, H. A. Weidenmuller, A. Gavron, J. R. Nix, and A. J. Sierk, Phys. Rev. C **34**, 209 (1986).

[46] I. Dioszegi, N. P. Shaw, I. Mazumdar, A. Hatzikoutelis, and P. Paul, Phys. Rev. C **61**, 024613 (2000).

[47] K. Mazurek, P. N. Nadtochy, E. G. Ryabov, and G. D. Adeev, Eur. Phys. J. A **53**, 79 (2017).

[48] J. P. Lestone, Phys. Rev. Lett. **70**, 2245 (1993).